PERIODIZED DAUBECHIES WAVELETS

JUAN MARIO RESTREPO
GARY K. LEAF
GEORGE SCHLOSSNAGLE

Mathematics and Computer Science Division
Argonne, National Laboratory, Argonne, IL 60439 U.S.A.

ABSTRACT. The properties of periodized Daubechies wavelets on $[0, 1]$ are detailed and contrasted with their counterparts which form a basis for $L^2(\mathbb{R})$. Numerical examples illustrate the analytical estimates for convergence and demonstrate by comparison with Fourier spectral methods the superiority of wavelet projection methods for approximations. The analytical solution to inner products of periodized wavelets and their derivatives, which are known as connection coefficients, is presented, and their use is illustrated in the approximation of two commonly used differential operators. The periodization of the connection coefficients in Galerkin schemes is presented in detail.

[1]. INTRODUCTION

Wavelets are finding a well-deserved niche in such areas of applied mathematics and engineering as approximation theory, signal analysis, and projection techniques for the solution of differential equations. While the concept of wavelets is not conceptually new [1] [2] [3], the past fifteen years have produced much of the theoretical underpinnings for the concept, as well as the generation of new wavelet families and the exploration of their potential in various areas of applied science [1] [2] [3] [4] [5].

Wavelets have several advantages: (1) they have compact support or exponentially decaying support; (2) their continuity properties may easily be increased, albeit at the expense of a larger domain of support; (3) for a given spline order, a complete basis may easily be generated by simple recurrence relations; (4) in the context of projection techniques, their convergence properties are as good as or better than Fourier methods, and they permit the analysis of extremely local functional behavior without the need for

Key words and phrases. wavelets, periodic, Galerkin, differential.

The authors thank John Weiss, of Aware, Inc., for making many preprints on the connection coefficients available to us. This research was supported in part by an appointment to the Distinguished Postdoctoral Research Program sponsored by the U.S. Department of Energy, Office of University and Science Education Programs, and administered by the Oak Ridge Institute for Science and Education. Further support was provided by the Atmospheric and Climate Research Division and the Office of Scientific Computing, U.S. Department of Energy, under Contract W-31-109-Eng-38. G. S. was a participant in the Summer 1993 Student Research Participation Program. This program is coordinated by the Division of Educational Programs, U.S. Department of Energy.

Typeset by $\mathcal{AMS}$-TEX

windowing and with little or no bias from global behavior; and (5) the manner in which the space is broken down into a family of multiply-enclosed subspaces enables spatial or temporal function multiresolution analysis.

To date, research has focused on compactly supported wavelets [**2**]; basic wavelets [**3**]; and smooth, exponentially decaying wavelets [**6**]. All of these wavelet families form a basis for $L^2(\mathbb{R})$. Work is currently under way on the generation of wavelets that are capable of spanning other classes of function space and/or domain. For example, Meyer [**3**] has shown how compactly supported wavelets can be made to form a basis for $L^2([0,1])$. He generates the periodized family by wrapping the $L^2(\mathbb{R})$ basis on a torus.

This report shows in detail how such a wrapping procedure is accomplished using Daubechies wavelets. The properties of the resulting wavelets on $L^2([0,1])$ are then contrasted with more standard Daubechies wavelets, which are now extremely popular in the signal processing community. This study also compares the convergence characteristics of periodized wavelet interpolation of functions with the characteristics of the Fourier spectral method.

The final section of this report is devoted to a derivation and numerical calculation of connection coefficients involving periodized Daubechies wavelets. Connection coefficients are matrix structures that result from the evaluation of inner products

$$\Omega_{j,k} \equiv \int \varphi_{j,k_0}^{(d_0)} \varphi_{j,k_1}^{(d_1)} ... \varphi_{j,k_n}^{(d_n)} dx,$$

where d_i is the number of differentiation with respect to x of the scaling function $\varphi = \varphi(x)$. Inner products arise naturally in the context of the Galerkin solution of differential equations. The name for these inner products was coined by Latto et al. [**7**], who developed a computational method that avoids the pitfalls of quadrature techniques. We use the technique of Latto et al. to calculate connection coefficients for the periodized Daubechies wavelets. A sample table of these coefficients appears in the appendix. Also included in the appendix is information on how to obtain these and other tabulated values of connection coefficients from the Mathematics and Computer Science Division at Argonne National Laboratory.

1.1 Wavelets and Multiresolution Analysis.

The value of wavelets hinges on their ability to perform multiresolution analysis. A multiresolution analysis is a nested sequence

$$V_0 \subset V_1 \subset ... \subset L^2(\mathbb{R})$$

satisfying the following properties:

(1) $\bigcap_{j\in\mathbb{Z}} V_j = 0$.
(2) $clos_{L^2}(\bigcup_{j\in\mathbb{Z}} V_j) = L^2(\mathbb{R})$.
(3) $f(x) \in V_j \Leftrightarrow f(2x) \in V_{j+1}$.
(4) There is a function $\varphi \in V_0$ such that $\{\varphi_{0,k}(x) = \varphi(x-k)\}_{k\in\mathbb{Z}}$ forms a Riesz basis for V_0.

The term φ is called the *mother scaling function* since, from (3), there exists $\{h_k\} \in l^2$ such that

$$\varphi(x) = \sqrt{2} \sum_{k \in \mathbb{Z}} h_k \varphi(2x - k).$$

This relation, called the *scaling relation*, will also hold for $\varphi(2x)$ and, by induction, for $\varphi(2^j x)$. In accordance with the notation in (4), we denote the translates and dilations of φ by

$$\varphi_{j,k}(x) = 2^{\frac{j}{2}} \varphi(2^j x - k).$$

The set $\{\varphi_{j,k}\}_{k \in \mathbb{Z}}$ forms a Riesz basis for V_j. We define W_j to be the orthogonal complement of V_j with respect to V_{j+1}. Just as V_j is spanned by dilations and translations of the mother scaling function, so are the W_j's spanned by translations and dilations of the *mother wavelet*. The mother wavelet is defined by

$$\psi(x) = \sqrt{2} \sum_k (-1)^{k-1} h_{-k+1+2M} \varphi_{1,k}(x),$$

with M a particular integer. Daubechies [2] constructed compactly supported wavelets and scaling functions using a finite set of nonzero $\{h_k\}_{k=0}^{N-1}$ scaling parameters with $N = 2M$ and $\sum_{k=0}^{N-1} h_k = \sqrt{2}$. With these scaling parameters, the recursion formulas generate the desired orthogonal wavelets and scaling functions with $supp(\varphi) = [0, N-1]$. Henceforth, these will be the wavelets we shall use, which we refer to as DN or Daubechies wavelets of order N. Values for φ are calculated using the scaling relation as indicated in the following procedure. First, the values it takes are determined at integer points. Then at the dyadic rationals at level 1 (the dyadic rationals at level j are $\mathbb{D}_j = \{\frac{k}{2^j}\}_{k \in \mathbb{Z}}$); using that information, we calculate the values at $\mathbb{D}N2$ and so on, until φ is defined at the dyadic rationals at all levels. Since the dyadics are dense in the reals, we simply extend φ continuously to $\mathbb{R}$. This procedure creates a function that is continuous but not differentiable for $DN = 4$, differentiable but not twice differentiable for $DN = 6$, and with increasing regularity for increasing DN [2]. The nature of the scaling relation guarantees that φ will be discontinuous in some derivative [8]. This procedure is easily accomplished computationally.

Another pleasing feature of these wavelets is their compact support. Whereas Fourier methods return global results, with compactly supported wavelets one can easily analyze short-lived events or pulses. Wavelet projection methods avoid distortion that might result from a local analysis with a windowed Fourier transform. As we shall see in the next section, compact support also makes the periodization of these wavelets an elegant process.

1.2 Other Properties of Wavelets.

In addition to items (1)–(4) mentioned above, wavelets have a number of other interesting properties. These will be given without proof. For further details, see Daubechies [2] or Chui [1].

(5) $\{\varphi_{j,k}\}_{j \geq 0, k \in \mathbb{Z}}$ is an orthonormal basis for $L^2(\mathbb{R})$.
(6) $V_{j+1} = V_j \bigoplus W_j$
(7) $L^2(\mathbb{R}) = clos_{L^2}(V_0 \bigoplus_{j=0}^{\infty} W_j)$.

(8) $\{\varphi_{0,k}, \psi_{j,k}\}_{j\geq 0, k\in\mathbb{Z}}$ is an orthonormal basis for $L^2(\mathbb{R})$.
(9) $\{\varphi_{j,k}, \psi_{l,k}; 0 \leq j \leq J \leq l, k \in \mathbb{Z}\}$ is an orthonormal basis for $L^2(\mathbb{R})$.
(10) $\int_{-\infty}^{\infty} \varphi(x)dx = 1$.
(11) $\sum_{k\in\mathbb{Z}} \varphi_{0,K} = 1$.
(12) $\int_{-\infty}^{\infty} \psi(x)x^k dx = 0 : k = 0, ..., M-1$.
(13) $\{x^k\}_{k=0}^{N-1} \in V_0$.

Item (6) is really the heart of multiresolution analysis and provides wavelet-based analysis with a distinctly different resolving quality in contrast to spectral methods: to go to a higher resolution of spatial scale, one simply adds on the next wavelet level (the next W_j) as implied by item (6). At some given level (say, with a representation in V_j), the multiresolution property *guarantees* all spatial scale information at all coarser levels. In contrast, with Fourier methods, information about one frequency gives no information about other frequencies.

[2]. Periodized Wavelets

The wavelets developed above are defined on $\mathbb{R}$. For many applications, however, wavelets defined on a periodic domain are needed. Interestingly, the wavelets defined above can be periodized with a Poisson summation technique to give periodic wavelets [2] that possess many of the same properties of their nonperiodic kin. Moreover, for large enough j, the periodization of $\varphi_{j,k}$ and $\psi_{j,k}$ is identical to their nonperiodic forms except for wrapping around the edges of the domain; and for large enough j, this too can be reduced to the nonperiodic case for most calculations. As would be expected, many of the above-mentioned properties are preserved in the periodic case as a result of the construction by the "scaling" property of the nonperiodic functions and their compact support.

The wavelets are periodized as follows:

$$\hat{\varphi}_{j,k}(x) \equiv \sum_{l\in\mathbb{Z}} \varphi_{j,k}(x-l) \text{ and } \hat{\psi}_{j,k}(x) = \sum_{l\in\mathbb{Z}} \varphi_{j,k}(x-l).$$

By construction $\hat{\varphi}$ and $\hat{\psi}$ are periodic and are well defined on $[0,1]$ since φ and ψ have compact support. Note that $\varphi_{j,k} = \varphi_{j,k'}$ if $k \equiv k' mod(2^j)$. Thus we shall restrict our attention to $0 \leq k < 2^j$. The same holds for the ψ's. In what follows, the properties of the periodic wavelets will be investigated in detail.

Periodized wavelet bases are not generated in quite the same way as the nonperiodic versions. In the nonperiodic case, bases are generated by repeated translation and dilation of the mother functions; but this approach is not possible in the periodic case because periodization does not commute with dilation. Therefore, the wavelet must be first dilated, then periodized. Although proof can be shown for the general case, we shall instead show that the elements in V_j for $j \leq 0$ are all constant functions. If dilation commuted with periodization, this would not be true.

Proposition. *For $j \leq 0$, $\varphi_{j,k} = 2^{\frac{-j}{2}}$.*

Proof. Since

$$\varphi_{j,k} = 2^{\frac{j}{2}}\varphi(2^j x - k),$$

then

$$\hat{\varphi}_{j,k} = \sum_{l\in\mathbb{Z}} 2^{\frac{j}{2}}\varphi(2^j(x-l)-k)$$
$$= 2^{\frac{j}{2}} \sum_{b=0}^{2^{-j}-1} \sum_{l\in\mathbb{Z}} \varphi(2^j x - (l+\frac{b}{2^{-j}}) - k).$$

Letting $y = 2^j x$ and summing over l, we obtain

$$\hat{\varphi}_{j,k} = 2^{\frac{j}{2}} \sum_{b=0}^{2^{-j}-1} 1 = 2^{\frac{-j}{2}}.$$

$\Diamond$

The most important property to be carried over to the periodized case is, of course, that the new functions form an orthonormal basis for $L^2[0,1]$.

Proposition. *$\{\varphi_{j,k} : j \geq 0, 0 \leq k < 2^j\}$ forms an orthonormal basis for $L^2[0,1]$.*

Definition:. $\langle f, g\rangle = \int f(x)g(x)dx$, the standard L^2 inner product.

Proof. We begin by showing that $\langle \hat{\varphi}_{j,k}, \hat{\varphi}j', k'\rangle = 0$:

$$\langle \hat{\varphi}_{j,k}, \hat{\varphi}j', k'\rangle = 2^{\frac{j+j'}{2}} \int_0^1 \sum_{l,l'\in\mathbb{Z}} \varphi(2^j(x-l)-k)\varphi(2^{j'}(x-l')-k')dx.$$

Let $y = x - l'$, so that

$$\langle \hat{\varphi}_{j,k}, \hat{\varphi}j', k'\rangle = 2^{\frac{j+j'}{2}} \int_0^1 \sum_{l,l'\in\mathbb{Z}} \varphi(2^j(x-l)-k)\varphi(2^{j'}(x-l')-k')dx$$
$$= 2^{\frac{j+j'}{2}} \int_{-l'}^{1-l'} \sum_{l,l'\in\mathbb{Z}} \varphi(2^j y + 2^j(l-l') - k)\varphi(2^{j'}y - k')dx$$
$$= 2^{\frac{j+j'}{2}} \sum_{r\in\mathbb{Z}} \int_{-\infty}^{\infty} \varphi(2^j y + 2^j r - k)\varphi(2^{j'}y - k')dx$$
$$= \sum_{r\in\mathbb{Z}} \langle \varphi_{j,k+2^j r}, \varphi_{j',k'}\rangle = \delta_{jj'}\delta_{kk'},$$

with $l - l' = r$. Thus $\hat{\varphi}_{j,k}$ and $\hat{\varphi}_{j',k'}$ are orthonormal. Next we show that they form a basis for $L^2[0,1]$.
Choose an arbitrary$f \in L^2[0,1]$. Now consider

$$\tilde{f}(x) = f(x)x \in [0,1] = 0x \notin [0,1].$$

$\tilde{f} \in L^2(\mathbb{R})$ and $\{\varphi_{j,k}\}$ form an orthonormal basis for $L^2(\mathbb{R})$, so we have $\tilde{f} = \sum_{\substack{0 \le j \\ k \in \mathbb{Z}}} \langle \tilde{f}, \varphi_{j,k} \rangle$ which, when periodized, becomes

$$f(x) = \sum_{l \in \mathbb{Z}} \tilde{f}(x-l) = \sum_{l \in \mathbb{Z}} \sum_{\substack{0 \le j \\ k \in \mathbb{Z}}} \langle \tilde{f}, \varphi_{j,k} \rangle = \sum_{\substack{0 \le j \\ k \in \mathbb{Z}}} \langle \tilde{f}, \hat{\varphi}_{j,k} \rangle.$$

This final result is actually a finite sum since, for $k \ge 2^j$ and $k \le 1-N$, $supp(\varphi_{j,k}) \cap supp(\tilde{f}) = \emptyset$. Thus f has a representation in the periodized wavelets.
$\Diamond$

The proof that $\{\hat{\varphi}_{j,k}, \hat{\psi}_{j',k} : j' \ge j \ge 0, 0 \le k < 2^j\}$ also form an orthonormal basis is nearly identical. Since $\varphi(x) = \sum_{k=0}^{N-1} h_k \varphi(2x-k)$, we can periodize both sides to get

$$\begin{aligned} \hat{\varphi}(x) &= \sum_{l \in \mathbb{Z}} \varphi(x-l) = \sum_l \sum_k h_k \varphi(2(x-l)-k) \\ &= \sum_k \sum_l h_k \varphi(2(x-l)-k) \\ &= \sum_k h_k \hat{\varphi}_{1,k}(x). \end{aligned}$$

Thus we have an orthonormal basis that still has a scaling relation. This means that in comparison with the nonperiodic case, we have a chain of spaces $\hat{V}_0 \subset \hat{V}_1 \subset \ldots \subset L^2[0,1]$ with the following properties:

(13) $\bigcup_{j \ge 0} \hat{V}_j = L^2[0,1]$ *with* $V_j = span\{\hat{\varphi}_{j,k}\}_{k=0}^{2^j-1}$.
(14) $\bigcap_{j \in \mathbb{Z}} \hat{V}_j = \{\text{constant functions}\}$.
(15) $f(x) \in V_j \Leftrightarrow f(2x) \in V_{j+1}$.
(16) By defining $\hat{W}_j = span\{\hat{\psi}_{j,k}\}_{k=0}^{2^j-1}$ we see that $\hat{W}_j$ is the orthogonal complement of $\hat{V}_j$ in $\hat{V}_{j+1}$. So then $clos(V_0 \bigoplus_{j=0}^{\infty} W_j) = L^2[0,1]$.

Clearly differences exist between the properties of the periodic case and the nonperiodic case. While they are both multiresolution spaces, the basis functions in the nonperiodic case are all formed by translations and dilations of the mother scaling function, φ, while in the periodic case it is often impossible to derive $\hat{\varphi}_{j+1}$ from $\hat{\varphi}_j$ (for example, consider $\hat{\varphi}_1$ and $\hat{\varphi}_0$; the latter is a constant function and thus unable to represent the former). It turns out, however, that there is no relation between $\hat{\varphi}_{j+1}$ and $\hat{\varphi}_j$ for very small j only. For j suitably large, the periodic case actually looks exactly the same as the nonperiodic case. This result is formalized as follows.

Proposition. *For $j \ge \log_2(N-1)$, $\hat{\varphi}_{j,0} = \varphi_{j,0}$, where $\hat{\varphi}$ is extended to $\mathbb{R}$ by setting it to 0 away from the unit interval.*

Proof. $supp(\varphi_{j,0}) = [0, 2^{-j}(N-1)]$, so for $j \ge \log_2(N-1)$, $supp(\varphi_{j,0}) = [0, \beta], \beta \le 1$. Thus $\hat{\varphi}_{j,0}(x) = \sum_{l \in \mathbb{Z}} \varphi_{j,0}(x-l) = \varphi_{j,0}$.
$\Diamond$

Thus, for large enough j, the periodization will affect the functions only by "wrapping them around" the edges of the domain. This is also a strong argument for using the scaling functions as trial-and-test functions when using periodized wavelets. By choosing j well, calculations can be performed as in the nonperiodic case; if desired, a multiresolution can then be performed easily. Calculations will not be so simple if $\hat{V}_0 \bigoplus_{k=1}^{j} \hat{W}_k$ is used as a test space, because, for low k, the basis for $\hat{W}_k$ is not equivalent to the basis for W_k.

[3]. Approximation Results and Methods

A function $f \in L^2[0,1]$ may be projected into the wavelet basis and expressed as $f = \sum_k a_{k_j} \hat{\varphi}_{j,k}$, where $a_{k_j} = \langle f, \hat{\varphi}_{j,k} \rangle$. Since the calculation of a_{j_k} is usually hard to evaluate analytically, numerical methods must be employed. In [9], a method was developed by using Taylor series expansions to approximate f. The method requires use of the moment equations to make $\mathcal{O}(h^n)$ approximations for $f \in C^n$. Unfortunately, in applications such as signal processing or any area where only a finite number of samples of f are provided, this method fails or requires interpolation. As an alternative, a function f given as samples on $\mathbb{D}_j \cap [0,1]$ may be approximated by a function $\tilde{f} \in \hat{V}_j$.

Define the samples of f as $\underrightarrow{f} \in \mathbb{R}$, with the k-th component of $\underrightarrow{f} = f(\frac{k-1}{2^j})$. Construct $\underrightarrow{\hat{\varphi}_{j,k}}$ from $\hat{\varphi}_{j,k}$ as shown previously. This yields, for $j > \log_2(N-2)$, a linearly independent spanning set for $\mathbb{R}^{2^j}$. Further, since $supp(\hat{\varphi}_{j,0}) = [0, 2^{-j}(N-1)$, $\underrightarrow{\hat{\varphi}_{j,k}}$ takes only $N-2$ values on $\mathbb{D}_j$, and $\underrightarrow{\hat{\varphi}_{j,k}}$ is just the k-th forward cyclic permutation of the elements of $\underrightarrow{\hat{\varphi}_{j,0}}$. The problem is thus reduced to finding the unique representation of $\underrightarrow{f}$ in terms of $\{\underrightarrow{\hat{\varphi}_{j,k}}\}_{0 \le k < 2^j}$, which is simply the solution of

$$A \underrightarrow{v} = \underrightarrow{f},$$

where A is the very sparse transformation matrix from the standard basis to the $\underrightarrow{\hat{\varphi}}$ basis. Define $\tilde{f}(x) = \sum_k \underrightarrow{v}(k) \hat{\varphi}_{j,k}(x)$. By construction, $\tilde{f}|_{\mathbb{D}_j} = f$.

In summary, this method involves solving the inverse problem with a sparse matrix, and results in a function $\tilde{f}$ with $\tilde{f}|_{\mathbb{D}_j} = f$. In essence, $\tilde{f}$ will be equal to f at all the sampled values.

We next show the manner in which the periodized wavelets may be used in the context of functional approximation. Since the wavelets form an orthonormal basis, the orthogonal projection operators onto V_j and W_j are defined respectively as

$$P_j(f) = \sum_{k=0}^{2^j-1} \langle f, \hat{\varphi}_{j,k} \rangle \hat{\varphi}_{j,k} \ , \ Q_j(f) = \sum_{k=0}^{2^j-1} \langle f, \hat{\psi}_{j,k} \rangle \hat{\psi}_{j,k}.$$

As we have already seen, periodized wavelets provide a basis for $L^2[0,1]$ so we have $\|f - P_j f\|_2 \to 0$, as $j \to \infty$. This is a property of any orthonormal basis of L^2, but this particular periodized basis has some additional properties.

Theorem. *If f is a continuous function on the torus, then $\|f - P_j f\|_\infty \to 0$ as $j \to \infty$.*

Proof. We begin the proof by showing that our projection operator is bounded. P_j is an integral operator of the form $P_j f(x) = \int_0^1 \sum_{k=0}^{2^j-1} \hat{\varphi}_{j,k}(y)\hat{\varphi}_{j,k}(x)f(y)dy$. Thus,

$$\begin{aligned}
\|P_j\|_\infty &\leq sup_{x\in[0,1]} \int_0^1 |\sum_{k=0}^{2^j-1} \hat{\varphi}_{j,k}(y)\hat{\varphi}_{j,k}(x)|dy \\
&\leq sup_{x\in[0,1]} |\sum_{k=0}^{2^j-1} \hat{\varphi}_{j,k}(x)| \|\hat{\varphi}_{j,k}\|_\infty [2^{-j}(N-1)] \\
&\leq sup_{x\in[0,1]} 2^{\frac{j}{2}} |\sum_{k=0}^{2^j-1} \hat{\varphi}(2^j x - k)| 2^{\frac{j}{2}} \|\hat{\varphi}\|_\infty 2^{\frac{j}{2}} [2^{-j}(N-1)] \\
&\leq sup_{x\in[0,1]} |\sum_{k=0}^{2^j-1} \hat{\varphi}(2^j x - k)| \|\hat{\varphi}\|_\infty (N-1).
\end{aligned}$$

Now, $|\sum_{k=0}^{2^j-1} \hat{\varphi}(2^j x - k)| < (N-1)\|\hat{\varphi}\|_\infty$ since for $j \geq \log_2(N-1)$ there are at most $(N-1)$ k's such that for a given x, $\{x\} \cap supp(\hat{\varphi}_{j,k}) \neq \emptyset$. Hence, we have

$$\|P_j\|_\infty \leq \|\hat{\varphi}\|_\infty^2 (N-1)^2.$$

If we take $f \in \bigcup_{j\in\mathbb{N}} V_j$, then $\exists J$ such that $\forall j \geq J, Q_j f = 0$. Thus, $P_j f = f$ for $j \geq J$. $\bigcup_{j\in\mathbb{N}} V_j$ is dense in $L^2[0,1]$ which is dense in $C(\mathbb{T})$, continuous functions of period 1 on the unit interval, Finally, by the boundedness of P_j, the theorem follows.
$\Diamond$

Theorem. *(Daubechies) If $f \in L^1[0,1]$, then $\|f - P_j f\|_1 \to 0$ as $j \to \infty$ [2].*

Proof. Since $L^1[0,1] \subset (C[0,1])^\star$, we have

$$\begin{aligned}
\|P_j f\|_1 &= sup\{|\langle P_j f, g\rangle|;\ \text{g continuous}\ , \|g\|_\infty \leq 1\} \\
&= sup\{|\langle f, P_j g\rangle|;\ \text{g continuous}, \|g\|_\infty \leq 1\} \\
&\leq \|f\|_1 \|P_j g\|_\infty.
\end{aligned}$$

$\|P_j\|_\infty$ is bounded by the previous theorem. Since $\bigcup_{j\in\mathbb{N}} V_j$ is dense in $L^2[0,1]$, which is also dense in $L^1[0,1]$, the uniform bound on P_j is sufficient to prove our result.
$\Diamond$

These two results are strong, in contrast to the convergence properties of Fourier functional approximations. In fact it has been shown that the continuous functions whose Fourier series do not uniformly converge are dense in $C(\mathbb{T})$ [**10**]. In this sense, wavelets provide a much more general basis than Fourier bases and hence have potentially broader applications.

These results suggest that wavelets should do a better job at pointwise approximation, especially for continuous functions. In Figures 1–4, we illustrate how wavelet and Fourier functional approximations compare with each other. The figures are graphs of the pulse function, $P(x) = e^{-1750(x-\frac{1}{2})}$, and the step function, $S(x) = \Xi_{[0,\frac{1}{2}]}$, against a 16-term ($V_4$) D_6 discrete wavelet approximation and against a 16-term discrete Fourier interpolation. These figures clearly show that for the C^∞ pulse function, the wavelets provide a much closer pointwise approximation. In fact, the only significant overshoot by the wavelets is at the base of the pulse. In contrast, the Fourier approximation shows a considerable amount of aliasing spread over the entire domain. Overshoot on the step function is confined to a neighborhood of the discontinuity. It is possible to resolve this inaccuracy with the wavelet techniques while maintaining a low number of approximating terms by continuing to take coarse approximations away from the discontinuity and projecting onto a finer scale in a neighborhood of the discontinuity. From these graphs we conclude that the finite-term wavelet functional interpolation is superior to its Fourier counterpart in approximating functions that contain a great deal of local information; moreover, it is better able to capture function discontinuities.

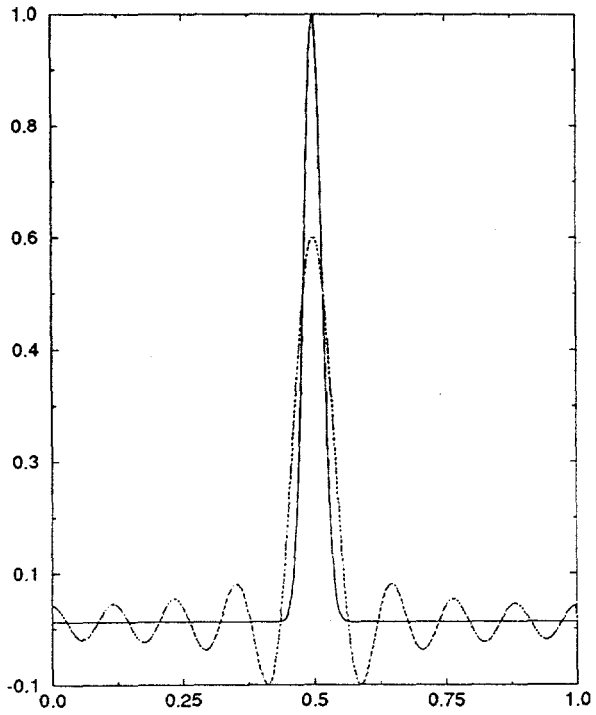

FIGURE 1. 16-term Fourier approximation to $P(x)$

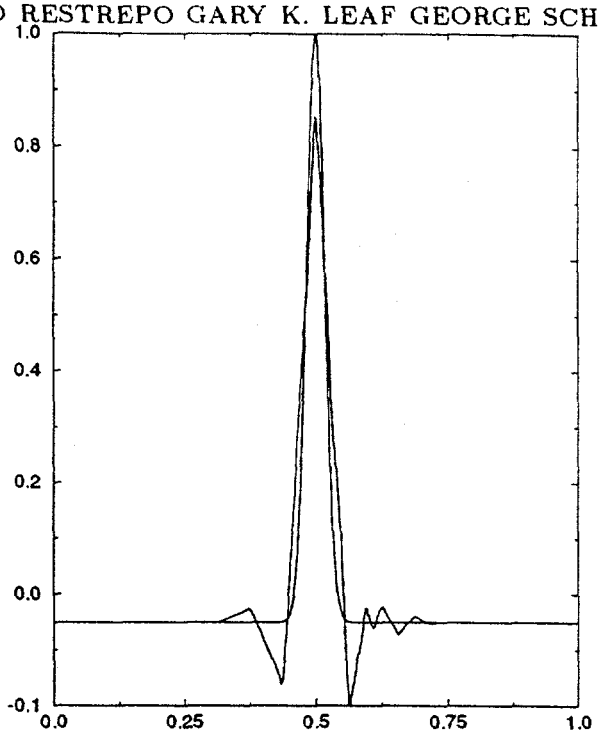

FIGURE 2. V_4 wavelet approximation to $P(x)$

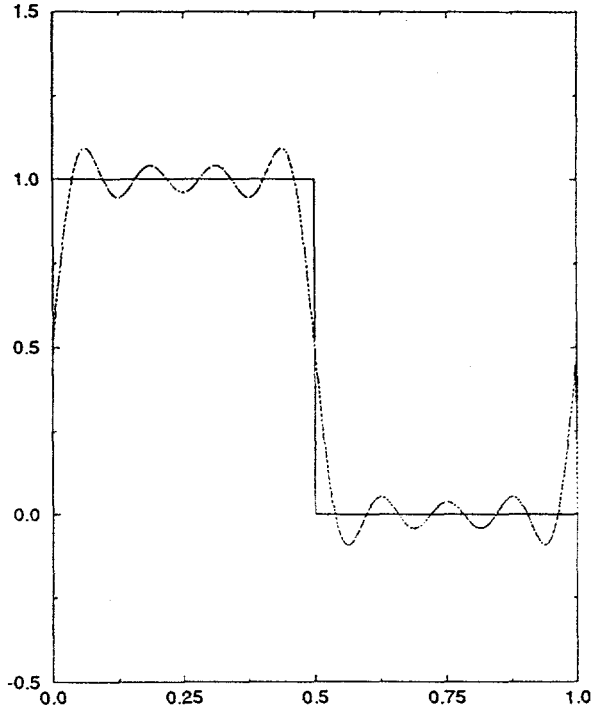

FIGURE 3. 16-term Fourier approximation to $S(x)$

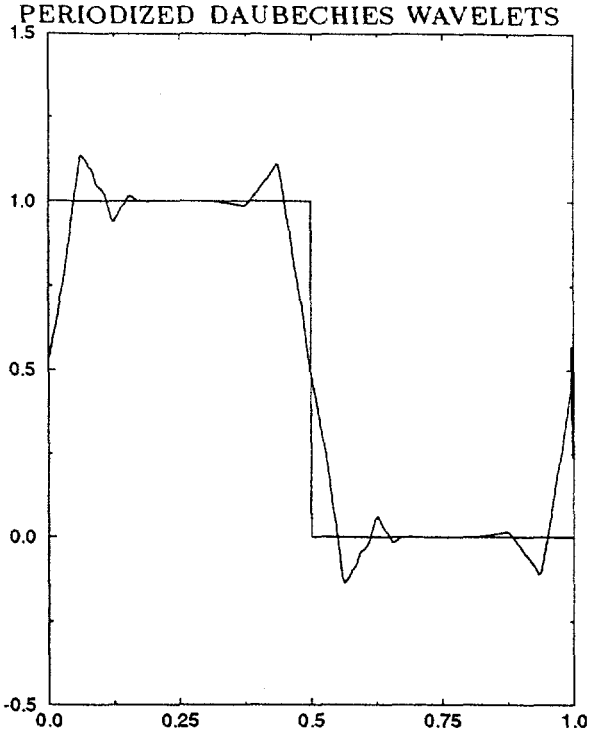

FIGURE 4. V_4 wavelet approximation to $S(x)$

To measure the error to which a truncated projection will approximate a desired function, we shall estimate its convergence. The natural choice of norms with which to measure convergence is the Sobolev norms. The sth Sobolev norm of a function f is defined as

$$\|f\|_{H^s} = (\int (1+x^2)^s \hat{f}^2(x)dx)^{\frac{1}{2}},$$

where H^s consists of those functions whose s Sobolev norm exists and is finite. Daubechies [**2**] states that the norm for H^s is equivalent to

$$\|f\|_{H^s[0,1]} = (\sum_{\substack{j\geq 0 \\ 0\leq k<2^j}} (1+2^{2js})\langle f, \hat{\psi}_{j,k}\rangle^2)^{\frac{1}{2}}.$$

Using this result, we easily find a bound for $\|f - P_p f\|_2$. For $f \in H^s[0,1]$,

$$\begin{aligned}
\|f - P_p f\|_2 &= \|\sum_{j\geq p0\leq k<2^j} \langle f, \hat{\psi}_{j,k}\rangle\|_2 \\
&= [\sum_{j,k}\langle f, \hat{\psi}_{j,k}\rangle^2]^{\frac{1}{2}} = [\sum_{j,k}\frac{2^{2js}}{2^{2js}}\langle f, \hat{\psi}_{j,k}\rangle^2]^{\frac{1}{2}} \\
&\leq [\sum_{j,k}\frac{2^{2js}}{2^{2ps}}\langle f, \hat{\psi}_{j,k}\rangle^2]^{\frac{1}{2}} \\
&= 2^{-ps}[\sum_{j,k} 2^{2js}\langle f, \hat{\psi}_{j,k}\rangle^2]^{\frac{1}{2}} \leq 2^{-ps}\|f\|_{H^s[0,1]}.
\end{aligned}$$

The same technique may be used to find error bounds in the H^l norm for $l \leq p$:

$$\begin{aligned}
\|f - P_p f\|_{H^l[0,1]} &= \Big(\sum_{\substack{j \geq p \\ 0 \leq k < 2^j}} (1 + 2^{2jl}) \langle f, \hat{\psi}_{j,k} \rangle^2 \Big)^{\frac{1}{2}} \\
&= \Big(\sum_{j,k} (1 + 2^{2jl}) \frac{(1 + 2^{2j(s-l)})}{(1 + 2^{2j(s-l)})} \langle f, \hat{\psi}_{j,k} \rangle^2 \Big)^{\frac{1}{2}} \\
&\leq (1 + 2^{2p(s-l)})^{-\frac{1}{2}} \Big(\sum_{j,k} (1 + 2^{2sj} \langle f, \hat{\psi}_{j,k} \rangle^2 \Big)^{\frac{1}{2}} \\
&\leq 2^{-p(s-l)} \|f\|_{H^s[0,1]}.
\end{aligned}$$

These bounds are similar to those on Fourier series [**11**]. As illustrated in Figures 5 through 8, numerical results confirm the similarity of convergence rates for wavelets and Fourier methods. In these figures the dashed curve represents the wavelet case. Figures 5 and 6 show the L^2 difference of $P(x)$ and $S(x)$ at dyadic points with their wavelet and Fourier approximations, as a function of the number of interpolants. The curves show that the convergence rates are of the same order.

Figure 5 also shows that for a lesser number of terms the two methods are comparable in capturing the features of a smooth pulse in the L_2, but as the number of terms is increased, the Fourier method supersedes the wavelet method. Figure 6 shows that the Fourier method is marginally better than the wavelet method for the step function. The change in the slope of Figure 5 is due to the spectral shape of $P(x)$: it is exponentially decaying whilst the step function has a spectrum that decays monotonically. As is well known, if the spectrum of a function has a finite rate of decay in k then this decay is observed after some k_o. If the Fourier interpolation is truncated below this threshold, the approximation will be very poor [**11**]. In Figure 5, the Fourier interpolation of $P(x)$ becomes acceptable with more than some 64 modes. In Figure 5, however, the Fourier approximation catches up to the monotonic decay of the spectrum of $S(x)$ quite quickly. Figures 7 and 8 show the L_1 approximation error. Figure 7 compares the error for the smooth pulse function $P(x)$; the wavelet case shows marginally better characteristics for a small number of interpolants, but the Fourier method is clearly superior for a larger number of modes. As could have been expected, for the less smooth step function $S(x)$ the situation is the reverse. For a larger number of wavelet interpolants the L_1 error is smaller than the Fourier counterpart, as is evident in Figure 8. Again, once the number of Fourier interpolants is over 64, say, the interpolation is substantially better for the $C^{\inf}$ pulse. For $S(x)$, however, the wavelet interpolation gets progressively better than the Fourier result.

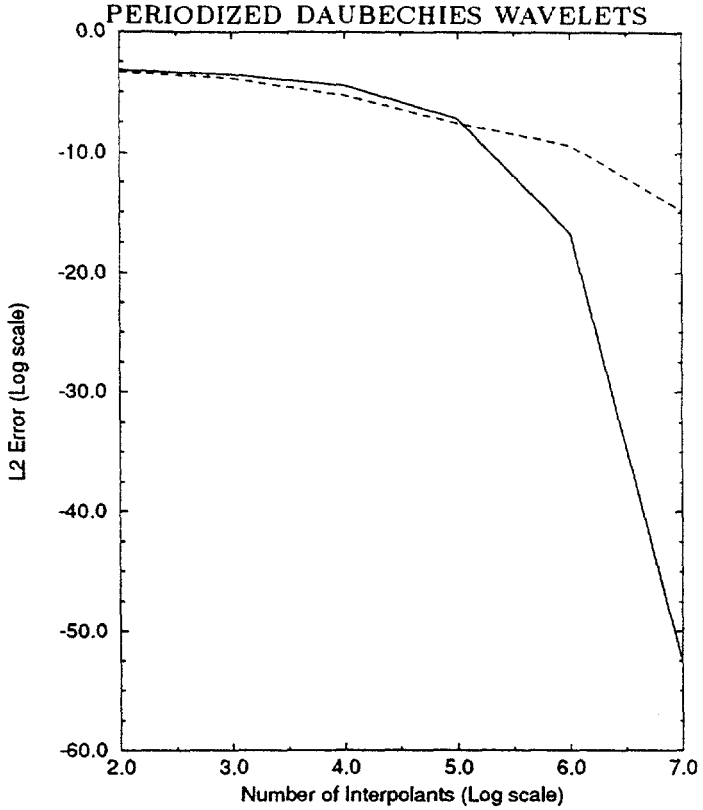

FIGURE 5. L^2 approximation error for $P(x)$. Dashed curve corresponds to the wavelet case.

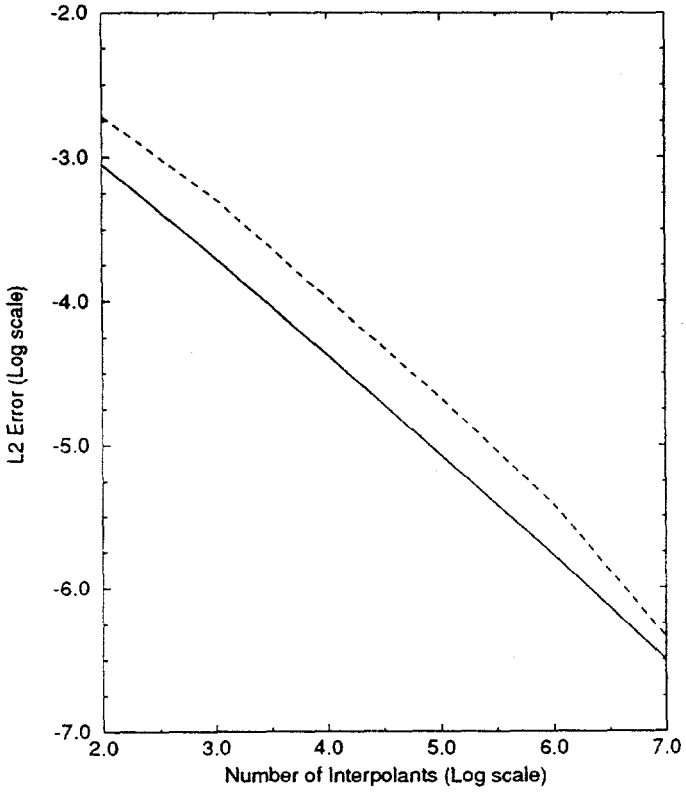

FIGURE 6. L^2 approximation error for $S(x)$. Dashed curve corresponds to the wavelet case.

To summarize, both methods produce comparable approximations to the two illustrative problems presented. For a small number of degrees of freedom, if one is interested in data compression applications, the wavelet method is slightly better than the Fourier method, in particular, for the C^∞ function. If an adequate number of Fourier interpolants is used, the Fourier method is better than the wavelet method. On the other hand, if the problem at hand requires the examination of the L_1 error, and the function has algebraic spectral decay, the wavelet method has a slight edge over the Fourier technique.

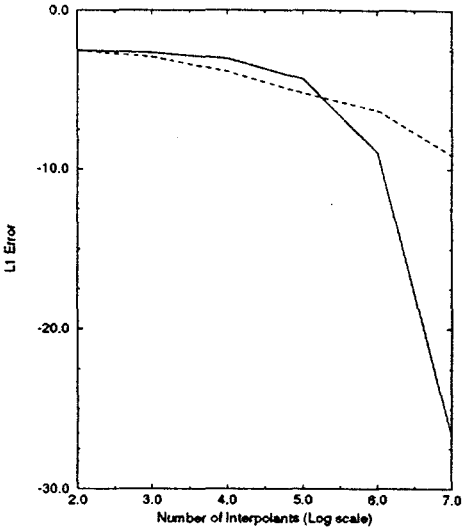

FIGURE 7. L^1 approximation error for $P(x)$. Dashed curve corresponds to the wavelet case.

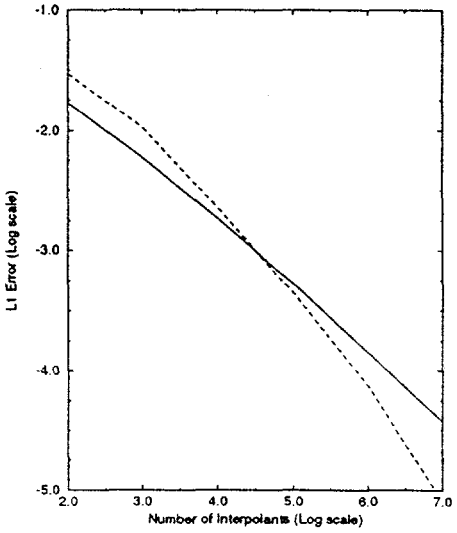

FIGURE 8. L^1 approximation error for $S(x)$. Dashed curve corresponds to the wavelet case.

[4]. METHODS FOR COMPUTING CONNECTION COEFFICIENTS

In wavelet applications, one often must represent operators in terms of wavelets [**12**]. An example of such an application is the Galerkin solution of differential equations. The

formulation of solutions will require integrations of the form

$$\Omega_{k_1,k_2,\ldots,k_n}^{d_1,d_2,\ldots,d_n} = < \varphi_{j,k_0}^{(d_0)} \varphi_{j,k_1}^{(d_1)} \ldots \varphi_{j,k_n}^{(d_n)} > = \int_0^1 \varphi_{j,k_0}^{(d_0)} \varphi_{j,k_1}^{(d_1)} \ldots \varphi_{j,k_n}^{(d_n)} dx,$$

where $\varphi^{(d)} = \frac{d^d \varphi}{dx^d}$. This expression is an n-term connection coefficient. Since φ cannot be represented in closed form for $DN > 2$ and, by construction, has limited regularity, analytic calculation of the integral is impossible, and numerical quadrature is often inaccurate as a result of the wildly oscillating nature of the resulting kernels. An alternative approach developed by Latto, Resnikoff, and Tenenbaum [7] circumvents some of the difficulty by exploiting the scaling relation and the moment condition to reduce the calculation to an eigenvector problem. Their method is designed for nonperiodic compactly supported wavelets. However, by invoking an extension of the earlier result regarding the equivalence of periodized and nonperiodized wavelets in Section 2, one may infer that for $j \geq \log_2((N-1)n)$, the periodized case yields the same result as the nonperiodized case. For illustration and for completeness in what follows we adopt closely the general procedure given in detail in [7] to the 2-tuple case. Several tabulated connection coefficients using periodized wavelets are included in the appendix of this study.

First, integration by parts is performed repeatedly on the above integral to obtain

$$\Omega_{k_1,k_2}^{d_1,d_2} = (-1)^{d_1} \Omega_{k_1,k_2}^{0,d_2+d_1},$$

where the periodicity of the wavelets has been invoked. By changing variables, we further reduce the equation to

$$\Omega_{k_1,k_2}^{0,d} = \Omega_{0,k_2-k_1}^{0,d} \equiv \Lambda_{k_2-k_1}^{d}, \text{ where } d = d_1 + d_2,$$

From these relations it is clear that any 2-tuple can be represented by a Λ_k^d.

To construct the eigenvector problem, fix d, then solve for $\{\Lambda_k^d\}_{0 \leq k < 2^j}$ by creating a system of 2^j homogeneous relations in Λ_k^d and enough inhomogeneous equations to reduce the dimension of the associated eigenspace to 1. Although we are using the connection-coefficient method for the nonperiodized case, we are computing them for the periodic case (by equivalence), which is where the bounds on k come into play.

4.1 Formation of Homogeneous Relations.

Fix d, $j \in \mathbb{N}$, such that $\varphi_j^{(d)}$ is well defined. To simplify notation, denote $\varphi_{j,k}^{(d)} \equiv \Phi_k^d$. In [7] it is suggested, without proof, that this method also holds for the first d for which Φ^d is discontinuous. For low-order differential equations, however, $DN = 6$ or $DN = 8$

wavelets should provide sufficient regularity. Since for every $0 \leq k < 2^j$,

$$\Lambda_k^d = \int \Phi_0(x)\Phi_k^d(x)dx = \int (\sum_{m=0}^{N-1} h_m \Phi_m(2x))(\sum_{l=0}^{N-1} h_l \Phi_{l+2k}^d(2x))2^d d(2x)$$

$$= 2^d \sum_m \sum_l h_m h_l \int \Phi_m(2x)\Phi_{l+2k}^d(2x)d(2x)$$

$$= 2^d \sum_m \sum_l h_m h_l \int \Phi_0(\zeta)\Phi_{l+2k-m}^d(\zeta)d\zeta, \text{ thus,}$$

$$\Lambda_k^d = 2^d \sum_{m=0}^{N-1}\sum_{l=0}^{N-1} h_m h_l \Lambda_{l+2k-m}^d.$$

In the above discussion, the integration is over the real line.

This linear homogeneous system can be represented as

$$A\underrightarrow{\lambda}^d = 2^{-d}\underrightarrow{\lambda}^d,$$

where $\underrightarrow{\lambda}^d = \{\Lambda_k^d\}_{0\leq k<2^j}$. It is worth noting here that if one needs to compute an n-tuple connection coefficient for $j < \log_2((N-1)n)$, then the periodic scaling relation can be used to resolve each $\varphi_{j,k}$ into the sum of $\varphi_{j',k}$'s with $j' \geq \log_2((N-1)n)$. Thus, the reduction to the nonperiodic case is a universally applicable method.

4.2 Generating Inhomogeneous Relations.

To generate the inhomogeneous equations, we must first assume $d \leq M-1$. The moment condition then guarantees that

$$x^d = \sum_{l\in\mathbb{Z}} \tilde{M}_l^d,$$

where $\tilde{M}_l^d = \langle x^d, \varphi_{0,l}\rangle$. Setting $x = 2^j\zeta$ and defining $M_l^d = \langle x^d, \Phi_l\rangle$, we have

$$\tilde{M}_l^d = 2^{dj}\dot{2}^{\frac{j}{2}}\langle \zeta^d, \Phi_l\rangle = 2^{dj}\dot{2}^{\frac{j}{2}} M_l^k.$$

This gives the relation

$$\zeta^d = \sum_{l\in\mathbb{Z}} M_l^d \Phi_l(\zeta),$$

which, when differentiated d times, yields

$$d! = \sum_{l\in\mathbb{Z}} M_l^d \Phi_l^d(\zeta).$$

Multiplying by Φ_0^0 and integrating, we obtain

$$\sum_{l\in\mathbb{Z}} M_l^d \int \Phi_0^0(\zeta)\Phi_l^d(\zeta)d\zeta = d!\int \varphi_{j,0}(\zeta)d\zeta = d!2^{\frac{-j}{2}}.$$

Thus $\sum_l M_l^d \Lambda_l^d = d! 2^{\frac{-j}{2}}$. The sum over l is actually over $|l| \leq N-2$ since the φ's are compactly supported. Thus, by changing the indices of summation by $m = l+1+(N-2)$, the inhomogeneous equations are

$$\sum_{m=1}^{2N-3} \Lambda_m^d M_{m-1-(N-2)}^d,$$

$$\text{with } M_l^d = 2^{\frac{-j(2d+1)}{2}} \tilde{M}_l^d.$$

The linear system formed by the 2^j homogeneous equations and the above inhomogeneous equations has eigenspace dimension equal to 1. Thus, all that remains to specify the system is to calculate $\tilde{M}_l^d$:

$$\begin{aligned} \tilde{M}_l^k = \int x^d \varphi(x-l)dx &= \int (y+n)^k \varphi(y)dy \\ &= \int \sum_{j=0}^{k} \binom{k}{j} y^j n^{k-j} \varphi(y)dy \\ &= \sum_{j=0}^{k} \binom{k}{j} n^{k-j} \tilde{M}_0^j. \end{aligned}$$

Since $\tilde{M}_l^0 = 1$ is a previously stated property of the φ, the above relation is used to evaluate recursively $\tilde{M}_l^d$ for all l.

The linear system is now complete and fixes the values of Λ_k^d. Note that while the scaling relation, which is used to generate the homogeneous relations, exists for periodized wavelets, currently nothing is analogous to the moment condition that may be used to generate the necessary inhomogeneous equations. One possible approach is to use the scaling equation linked with the fact that $\hat{V}_j = \{\text{constant functions}\}$ for $j \leq 0$ to find additional inhomogeneous relations. Problems arise with relating $\int \hat{\varphi}_{j+1,0} dx$ to $\int \hat{\varphi}_{j,0} dx$, however, since dilation does not commute with periodization. While this method could probably be worked out, the periodic case can always be reduced to an equivalent nonperiodic case for which the method is already well defined. Thus, to compute an n-term connection coefficient for periodized wavelets, one need only resolve the terms into $\hat{V}_j$, for some $j \geq \log_2(N-1)n$ and apply the above method. This approach takes full advantage of the equivalence of periodic and nonperiodic scaling functions and circumvents the need for a connection coefficient method particular to periodized wavelets.

4.3 Periodization of Inner Product Matrices.

The two most common situations that arise in the wavelet Galerkin solution of differential equations involve 2-tuples and 3-tuples. Periodic conditions require wraparound of the Λ entries in Ω in the upper right-hand corner and the lower left-hand corner, assuming that the matrix row index increases from top to bottom corresponding to the dyadic points in $[0,1)$. The wraparound will produce at most $N(N+1)$ additional entries in the

matrix, where $[0, N]$ is the support of the scaling functions. In this section we present explicit schemes that enable the construction of these matrices. The 2-tuple case is easily generated, since Ω is a circulant matrix of the form

$$\Omega = \text{circ}(\Lambda_0, \Lambda_1 \ldots \Lambda_N, 0, \ldots \Lambda_{-N}, \Lambda_{-N+1}, \ldots \Lambda_{-1})$$

and $\Omega = \pm\Omega^T$, depending on whether the operator is symmetric or skew-symmetric (see Section **4.5**).

The 3-tuple is somewhat more involved. The $\Lambda_{j'',k''}$ have the structure illustrated schematically in Figure 9a. We call this structure the "index pad." Let $K = 2^p - 1$, where the superscript p corresponds to the resolution of the scaling functions. A typical situation in a Galerkin discretization when 3-tuples are involved would be the calculation of

$$s_k = \sum_{l=0}^{K} a_l \omega_{k,l}$$

$$\text{where } \omega_{k,l} = \sum_{j=0}^{K} h_j \Omega_{k,j,l},$$

where a_l and h_j are the wavelet coefficients of the projection of real quantities $A(x,\cdot)$ and $H(x,\cdot)$ into V^p, and Ω is the inner product $< \phi_k^{d_1} \phi_j^{d_2} \phi_l^{d_3} >$. For a given k there is an index pad in (j,l) over which these indices range when forming $\omega_{k,l}$ and s_k. Moreover, associated with each index (j,l) in the pad there is a $\Lambda_{j'',k''}$, where $j'' = j - k$ and $l'' = l - k$, which gives the value of $\Omega_{k,j,l}$. It is easier to think of the index pad as having a rectangular structure in which the entries lying outside of the hexagon of the true index pad are zero.

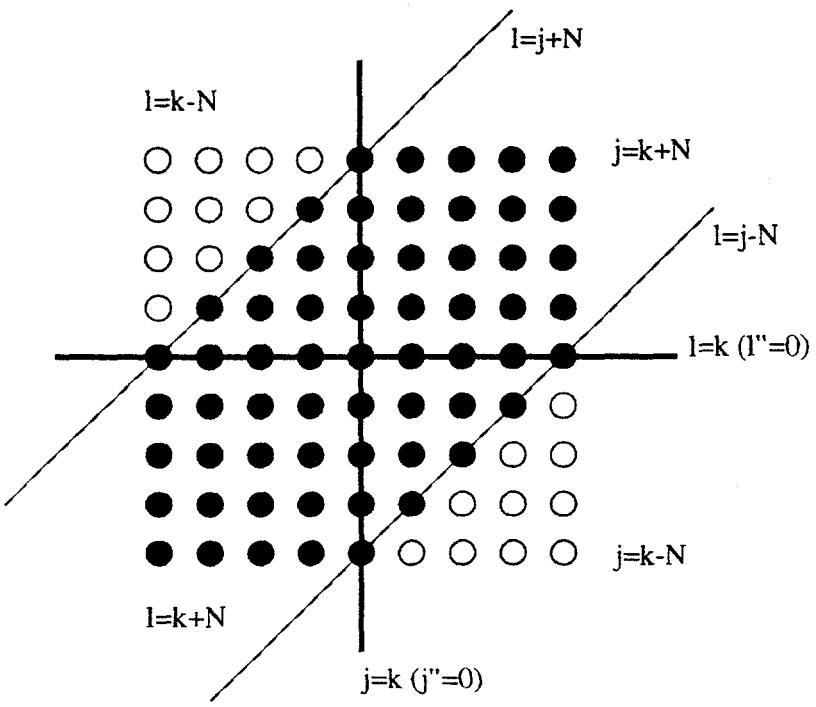

FIGURE 9A. Structure of $\Lambda_{j'',k''}$ index pad for 3-tuples in the (j,l)

plane. The index pad corresponds to $N = 4$ in the region where no wraparound arises.

First consider the case in which there is no wraparound, that is, for $N \leq k < k'$, where $k' = K - (N-1)$, the largest index k for which the support of the scaling function lies entirely in $[0,1]$. Associated with each (j'', l'') in the index pad, there is a connection coefficient $\Lambda_{j'',l''}$. As k is varied, the pad centered at k, moves along the line $l = j$ in the (j,l) plane. This is the "regular case" and is shown in Figure 9a.

Next, consider the case $k \geq k'$. Let $k = k' + \sigma$, $0 \leq \sigma \leq N-1$. The situation is illustrated in Figure 9b. The index pad is beyond $(j,l) = (K,K)$. For convenience identify the following subregions.

$$
\begin{aligned}
A :& k - N \leq j \leq K \\
& k - N \leq l \leq K \\
B :& j = K + 1 + q, 0 \leq q \leq \sigma \\
& l = K - t, 0 \leq t \leq N - 1 \\
C :& j = K - t, 0 \leq t \leq N - 1 \\
& l = K + 1 + q, 0 \leq q \leq \sigma \\
D :& j = K + 1 + q, 0 \leq q \leq \sigma \\
& l = K + 1 + q, 0 \leq q \leq \sigma.
\end{aligned}
$$

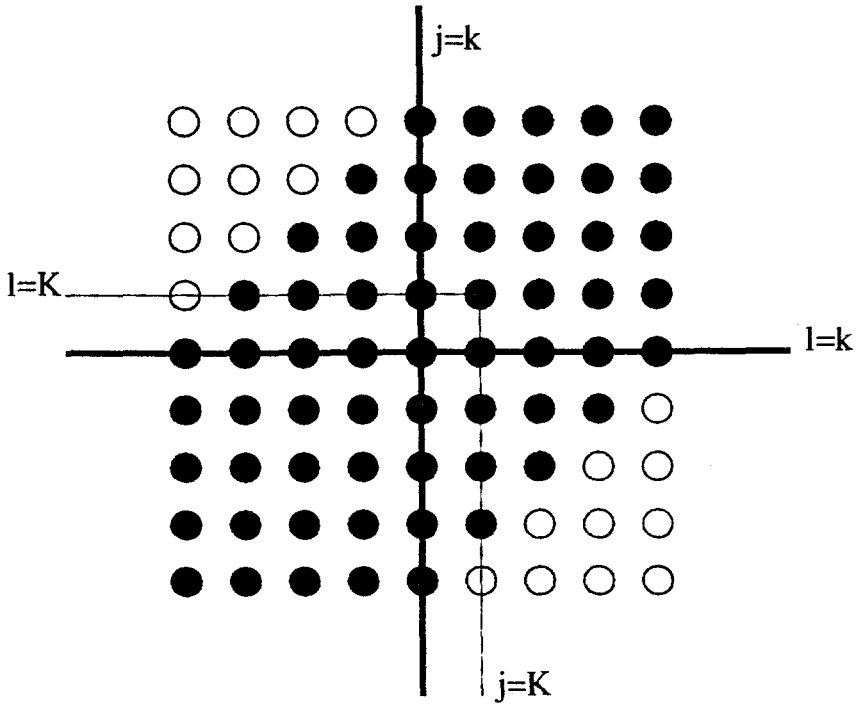

FIGURE 9B. Structure of $\Lambda_{j'',k''}$ index pad for 3-tuples in the (j,l) plane corresponding to $N = 4$ for $k = k' + 2$

Consider a given k, the corresponding index pad is subdivided into the four subsets A, B, C, D defined above. When index pairs (j,l) lie in subregions B, C, or D, periodization comes into play since the corresponding basis functions have been periodically extended. We now consider the consequences of this periodization on the s_k in detail. Note that s_k will be the sum of three partial sums, summed over subsets of the index pad. Next we observe that the range of l is $k-N \le l \le K+1+\sigma$. We divide this range into two parts: $k-N \le l \le K$ and $K+1 \le l \le K+1+\sigma$. For the range $k-N \le l \le K$, the index l is not affected by the periodization since $l \le K$. The index j, on the other hand, produces a pair (j,l) that ranges over the set A and B. Let $\omega_{k,l} = \omega^r_{k,l} + \omega^p_{k,l}$. Then

$$\omega^r_{k,l} = \sum_{j=k-N}^{K} h_j \Lambda_{j'',l''} \text{ , the regular part,}$$

$$\omega^p_{k,l} = \sum_{j=K+1}^{K+1+\sigma} h_{j-K-1} \Lambda_{j'',l''} \text{ , the periodic adjustment, and thus}$$

$$s^{(1)}_k = \sum_{l=0}^{K} a_l \omega_{k,l},$$

where, throughout this section, we set $j'' = j-k$ and $l'' = l-k$.

Next we deal with the range $K+1 \le l \le K+1+\sigma$. In this case the pair $(j,l) \in C \cup D$. When $(j,l) \in C$,

$$\omega_{k,l} = \sum_{j=k-N}^{K} h_j \Lambda_{j'',l''}.$$

Now the index l is affected by periodization, so that

$$s^{(2)}_k = \sum_{l=K+1}^{K+1+\sigma} a_{l-K-1} \omega_{k,l}.$$

When $(j,l) \in D$, both indices are affected by periodization, thus

$$\omega_{k,l} = \sum_{j=K+1}^{K+1+\sigma} h_{j-K-1} \Lambda_{j'',l''}.$$

Then,

$$s^{(3)}_k = \sum_{l=K+1}^{K+1+\sigma} a_{l-K-1} \omega_{k,l}.$$

So, for $k = k' + \sigma$, $0 \le \sigma \le N-1$, combining, we have

$$s_k = s^{(1)}_k + s^{(2)}_k + s^{(3)}_k.$$

We now consider the case when the index pad encounters the left boundary, $j = 0$, $l = 0$, which occurs for $0 \leq k \leq N-1$. Schematically, the situation is portrayed in Figure 9c. Denote the following subregions

$$\begin{aligned} A &: 0 \leq j, l \leq k+N \\ B &: 0 \leq l \leq N-1 \\ &\quad -\sigma - 1 \leq j \leq -1 \\ C &: 0 \leq j \leq N-1 \\ &\quad -\sigma - 1 \leq l \leq -1 \\ D &: -\sigma - 1 \leq j \leq -1 \\ &\quad -\sigma - 1 \leq l \leq -1, \end{aligned}$$

where $0 \leq \sigma \leq N-1$.

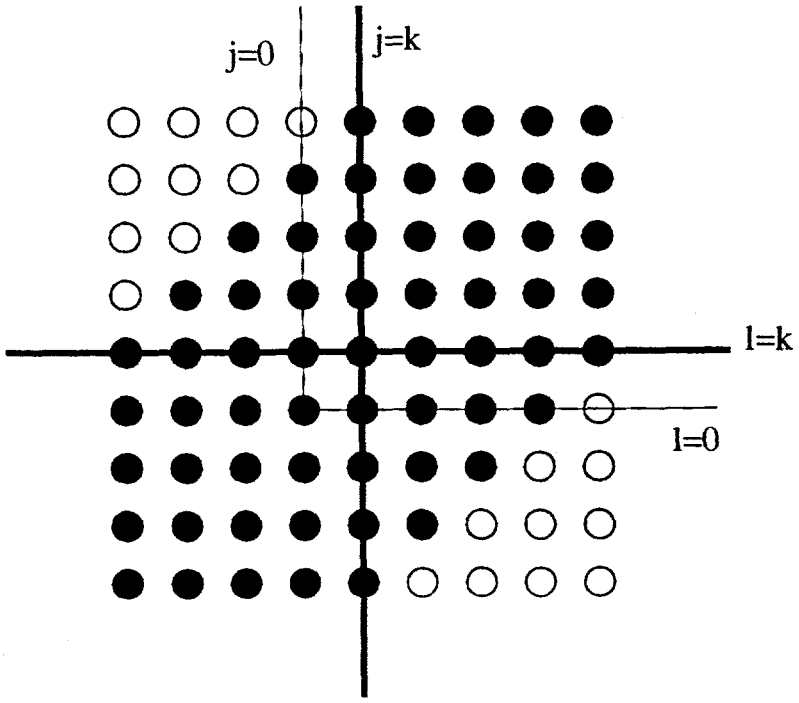

FIGURE 9c. Structure of $\Lambda_{j'',k''}$ index pad for 3-tuples in the (j,l) plane corresponding to $N = 4$ for $k = N-3, \sigma = 2$

Again we divide the entire l range $-\sigma - 1 \leq l \leq k+N$ into two parts: $0 \leq l \leq k+N$ and $-\sigma - 1 \leq l \leq -1$. Consider the range $0 \leq l \leq k+N$ for which the index pair (j,l) ranges over B and A. When $(j,l) \in B$, the index j is affected by periodization so that $\omega_{k,l}$

has a regular part and a periodic part. Let $\omega_{k,l} = \omega^r_{k,l} + \omega^p_{k,l}$. Then

$$\omega^r_{k,l} = \sum_{j=0}^{k+N} h_j \Lambda_{j'',l''} \text{ , the regular part, and}$$

$$\omega^p_{k,l} = \sum_{j=-\sigma-1}^{-1} h_{K+1+j} \Lambda_{j'',l''} \text{ ; thus}$$

$$s^{(1)}_k = \sum_{l=0}^{k+N} a_l \omega_{k,l}.$$

Next we deal with the range $-\sigma - 1 \leq l \leq -1$. In this case $(j,l) \in C \cup D$. For $(j,l) \in C$, we have

$$\omega_{k,l} = \sum_{j=0}^{N-1} h_j \Lambda_{j'',l''}.$$

$$\text{Then } s^{(2)}_k = \sum_{l=-\sigma-1}^{-1} a_{K+1+l} \omega_{k,l}.$$

When $(j,l) \in D$ we have

$$\omega_{k,l} = \sum_{j=-\sigma-1}^{-1} h_{K+1+j} \Lambda_{j'',l''}$$

$$\text{and } s^3_k = \sum_{l=-\sigma-1}^{-1} a_{K+1+l} \omega_{k,l}.$$

Combining, for $k = N - \sigma - 1$, $0 \leq \sigma \leq N - 1$, we have

$$s_k = s^{(1)}_k + s^{(2)}_k + s^{(3)}_k.$$

The periodization is then complete. The result is the vector $\{s_k\}$. This procedure generalizes to the n-tuple case in a straightforward manner.

4.4 Useful Connection Coefficient Relations.

We list a number of identities and relations that are useful in the manipulation of connection coefficients. Many of these relations appear in [7] and [13]. Except for the operator inversion relationship, most of the inner product relations can easily be derived

by invoking integration by parts, translation, and change of variables.

$$\Omega_{l,m}^{d_1,d_2} = \Omega_{m,l}^{d_2,d_1} \tag{17}$$

$$\Lambda_l^{d_1,d_2} = -\Lambda_l^{d_1-1,d_2+1} \tag{18}$$

$$\Lambda^{d_1,d_2,d_3} = -\Lambda^{d_1-1,d_2+1,d_3} - \Lambda^{d_1-1,d_2,d_3+1} \tag{19}$$

$$\Lambda_{l,m}^{d_1,d_2,d_3} = \Lambda_{-l,m-l}^{d_2,d_1,d_3} \tag{20}$$

$$\Lambda_{l,m}^{d_1,d_2,d_3} = \Lambda_{l-m,-m}^{d_3,d_2,d_1} \tag{21}$$

$$\Lambda_{l,m}^{d_1,d_2,d_3} = (-1)^{d_1} \sum_{i=0}^{d_1} \binom{d_1}{i} \Lambda_{l,m}^{0,d_2+i,d_3+d_3+d_1-i}. \tag{22}$$

Another relation that is very useful in checking the construction and accuracy of 3-tuple matrices is the check-sum procedure: the column sum of a 3-tuple matrix must equal a corresponding 2-tuple vector component for component. For example, $\sum_{l=0}^{K} \Omega_{l,m}^{1,0,0} = \Omega_m^{1,0}$.

Lastly, we mention an efficient procedure for the inversion of a first order operator, which exploits the symmetric or skew-symmetric nature of the matrix, $\Omega = \pm\Omega^T$, so that the matrix may be diagonalized, $\Omega = \Phi D_\Omega \Phi^T$. A concrete example of operator inversion appears in [**13**].

[5] Approximation of Differential Operators

The spectrum $\{\sigma_j\}$ of the continuous differential operator $\mathcal{L}$ with periodic boundary conditions on 0 and 1 is discrete. A discrete approximation L of the operator may be found by projecting the operator onto the space spanned by the periodized scaling functions. The discrete and continuous operators can be compared by looking at their spectra. By the Galerkin procedure outlined in Section 4.3 one can form the matrix Ω, an approximate representation of L, in the subspace of periodized scaling functions of resolution p and of order DN. In this section we examine the usefulness and properties of wavelet projection techniques for differential operators.

The projection of the differential operator with periodic boundary conditions leads to a 2-tuple Ω. Eigenvalues of this matrix may be found by two different methods: the circulant matrix Ω, once constructed, can then fed into an eigenvalue solver (ES); alternatively, one can make use of the fact [**14**] that the eigenvalues λ of a circulant matrix (EC) are given by the expression

$$\lambda_j = \sum_{k=0}^{K} a_k \exp^{\frac{i2\pi kj}{K}},$$

where a_k is an entry in the first row in the circulant matrix, namely, an element of the set $\Lambda_0, \Lambda_1 \ldots \Lambda_N, 0, \ldots \Lambda_{-N}, \Lambda_{-N+1}, \ldots \Lambda_{-1}$, and $j = 0, 1, \cdots, K$. In the course of the discussion on approximations to differential operators, qualitative differences between both methods will be briefly explored.

The most important difference in the eigenvalue finding strategies is that the numerical accuracy of EC is controlled solely by the accuracy in the calculation of the Λ's whereas in

TABLE 1. Residual for the least-squares calculation of Λ's used in $\Omega^{0,1}$, as a function of p and DN

DN	p	Residual
4	4	-2.1926904736347D-15
4	5	-8.4099394115356D-15
4	6	-8.3266726846887D-15
4	7	-2.6922908347160D-14
4	8	-2.1510571102112D-16
6	4	4.3905851176973D-15
6	5	4.3905851176973D-15
6	6	2.2332830029725D-14
6	7	3.2980562725271D-14
6	8	-1.6563139748627D-14
8	4	-1.6766260279716D-11
8	5	-3.3533817109376D-11
8	6	6.7080697513231D-11
8	7	1.3417001243474D-10
8	8	2.6830899981444D-10

ES the accuracy is further controlled by the eigenvalue solver. The Λ's were obtained by the procedure outlined in the preceding section. The overdetermined system was solved using a QR algorithm from LAPACK [**15**]. For $\Omega^{0,1}$, the residual as a function of the resolution p and the order DN appears in Table 1.

The eigenvalues of $\Omega^{0,1}$ calculated using the ES method are plotted as a function of p in Figure 10a. The same calculation using the EC expression appears in Figure 10b. The eigenvalues found using ES are complex conjugate, those found using EC are not. The computation was performed in double precision using a standard eigenvalue solver from LAPACK. Four sets are plotted: in increasing magnitude, they correspond to $p = 4, 5, 6, 7$. Regarding these figures, one can make three important observations. First, the imaginary part of the eigenvalues grows only as $O(K)$, in sharp contrast to a spectral approximation based on Chebychev bases. Second, we observe that the real parts of the eigenvalues are comparable to the size of machine precision, again in sharp contrast to Chebychev and Legendre bases investigated by Trefethen *et al.* [**16**]. Third, we saw little evidence of contamination due to round-off error even for high resolution (in our experiments, we tried values of p as high as 11), in sharp contrast to the experience of Trefethen *et al.* with the above-mentioned bases functions.

The spectrum of the skew-symmetric operator $\frac{d}{dx}$ is purely imaginary and equal to $2\pi k$, where $k \in \mathbb{Z}$. Periodicity will lead to the eigenvalue 0 having multiplicity 2. Table 2 shows the magnitude of the imaginary part of the first few EC eigenvalues, divided by 2π, as

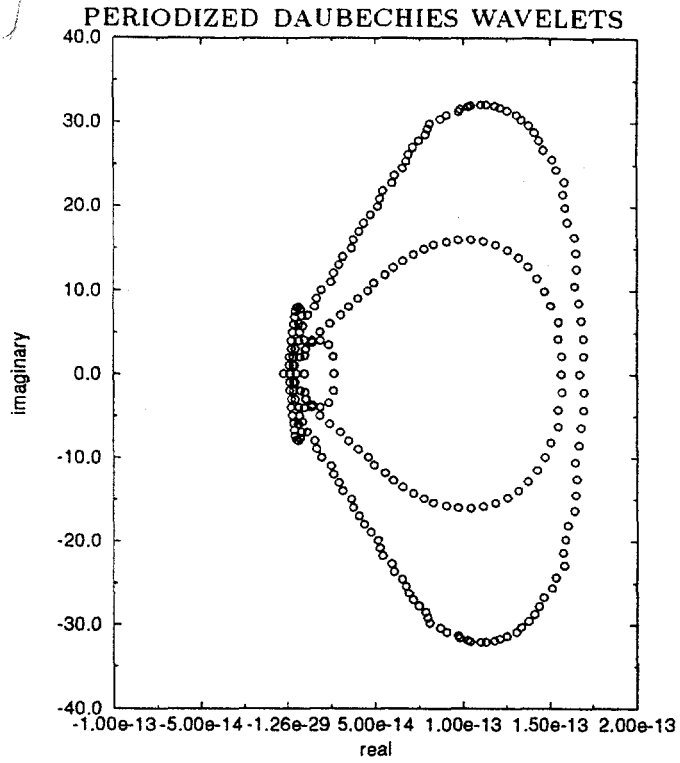

FIGURE 10A. ES approximation to the spectrum of $\frac{d}{dx}$. In increasing magnitude, for $p = 4, 5, 6, 7$. $DN = 6$. Note the scale discrepancy between axes.

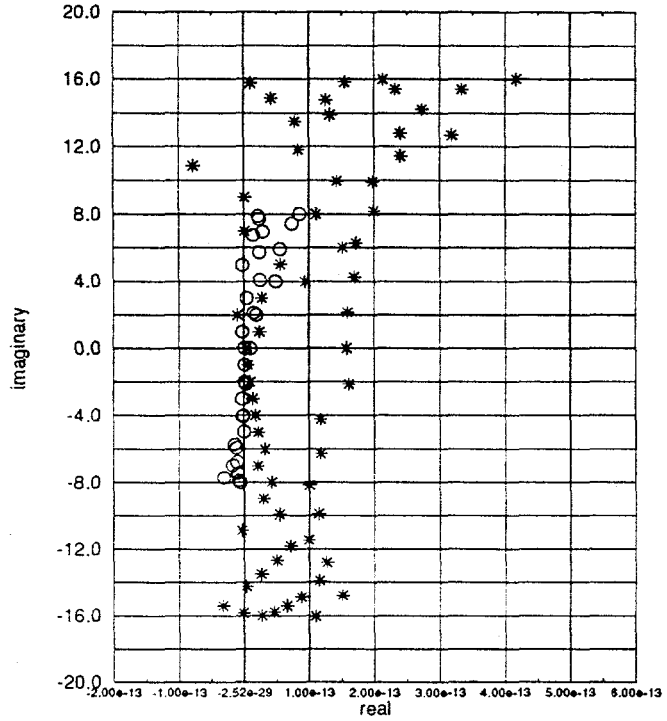

FIGURE 10B. EC approximation to the spectrum of $\frac{d}{dx}$ for two different resolutions. $p = 5$ (circles) and $p = 6$. $DN = 6$ (stars)

a function of p. It is clear from the table that approximations to the eigenvalue improve

TABLE 2. Eigenvalues divided by 2π for increasing resolution $K = 2^p$ calculated with the EC method. $DN = 6$

$p = 4$	$p = 6$	$p = 8$
0.0D0	0.0D0	0.0D0
0.99997222310553	0.99999999300555	0.99999999999689
1.9967784015701	1.9999991102504	1.9999999997795
2.0423307943545	2.9999849535965	2.9999999962590
2.9532542889943	3.9998888924219	3.9999999720194
3.4758292699748	4.9994799193486	4.9999998667457·
3.7208826878105	5.9981781285634	5.9999995232107
4.0025895152829	6.9947814463569	6.9999985996877

TABLE 3. Real and imaginary parts of eigenvalues of $\frac{d}{dx}$ as a function of DN for $p = 6$. Real and imaginary pairs are listed in consecutive rows

$DN = 4$	$DN = 6$	$DN = 8$
0.99999690699928	0.99999999300555	0.99999999998407
1.4701230527654D-14	2.3748141621594D-14	2.0355549961367D-14
1.9999013641150	1.9999991102504	1.9999999916456
-1.6962958301139D-14	-1.0177774980683D-14	-1.5832094414396D-14
2.9992552692402	2.9999849535965	2.9999996834005
1.5832094414396D-14	2.7140733281822D-14	1.9224686074624D-14

as p is increases and the number of reasonably correct eigenvalues grows as well with p. Parenthetically, we remark that with $p = 6$ we can go as far $k = 11$ for which $\lambda_{11} \doteq 10.8$ while retaining at least one digit of accuracy. In the case $p = 8$ we can go as far as $k = 36$ for which $\lambda_{36} \doteq 35.8$.

We examined the dependence of the eigenvalue convergence on both the resolution p and the order DN. We did this by examining the imaginary part of several eigenvalues. We found that the rate of convergence was almost exactly 2^{-p}, while the dependence of the rate of convergence on DN was essentially quadratic. Table 2 and Table 3 illustrate the above-mentioned rates of convergence.

For the ES method we found that when p increases beyond 7, the eigenvalues trace the same figure as when smaller values of p are used; however, while the real part was strictly positive for $p \leq 7$, the real part can be strictly positive for $p \geq 8$. We did not try cases beyond $p = 9$. When the same calculation is performed in single-precision arithmetic, the same sign reversal of the real part occurred for the same values of p. The outcome is shown in Figure 11a. The flattened elliptical pattern in Figures 10a and 11a is due to periodization. Figure 11b compares the computation of the $\frac{d}{dx}$ operator with periodic

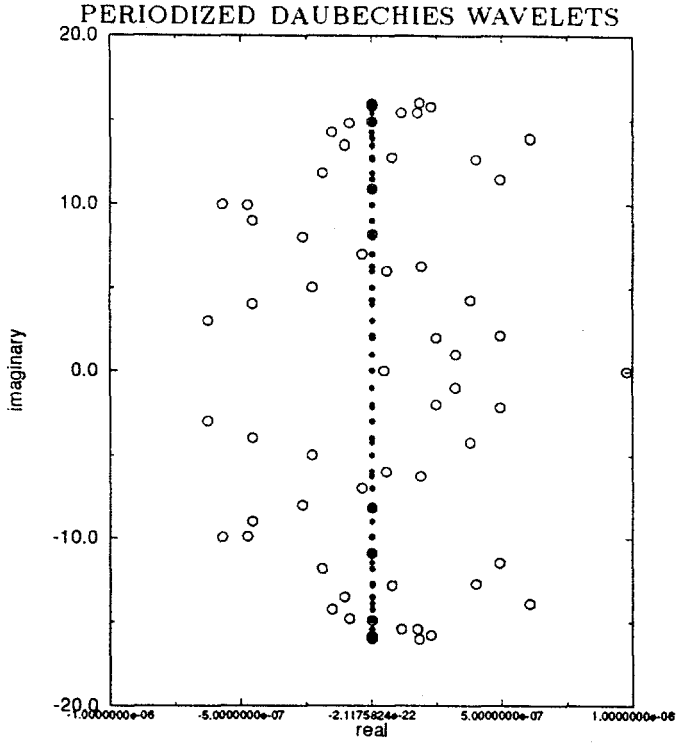

FIGURE 11A. ES single-precision (circles) versus double-precision (stars) spectrum calculation of $\frac{d}{dx}$: $p = 6$

boundary conditions with this condition removed. The effect of removing the periodicity terms in the operator matrix changes the pattern in the graphs of the eigenvalues, however, reversal still occurs.

Qualitatively, we find the same type of behavior in higher odd-ordered differential operators. Figure 12 shows the ES approximation to the spectrum of the operator $\frac{d^3}{dx^3}$ with periodic boundary conditions. The reversal in the eigenvalues as a function of p occurs for p much smaller than in the first derivative calculation. Moreover, we find the rates of convergence very similar to those of the first derivative, with the proviso that the basis functions had to be chosen with sufficient smoothness.

Finally we consider approximation to even-ordered differential operators. For example, Figure 13a shows the ES spectrum of $\frac{d^2}{dx^2}$ for periodic boundary conditions for the same values of p. This case corresponds to the eigenvalues of $\Omega^{0,2}$. Each eigenvalue has a complex conjugate, for which the imaginary part is slightly higher than machine precision. The qualitative differences between the ES and EC methods in the calculation of $\frac{d^2}{dx^2}$ are shown in Figure 13b.

Again, we found the same rates of convergence as in the odd-ordered cases. Table 4 lists the real part of the eigenvalues as a function of p, as given by the EC method.

Using the eigenvalue data corresponding to the three differential operators, we have also been able to assess numerically the size of the largest eigenvalues. This is a useful estimate, for example, in the determination of time stability in numerical schemes for the solution of differential equations. The estimate is that the largest eigenvalue is comparable in size to Fourier spectral approximations; that is, the largest eigenvalue $\nu/(2\pi)^n = O(K^n)$, for $\frac{d^n}{dx^n}$, where $n = 1, 2, 3$, when $K = 2^p$ is large. For small K this is an overestimate.

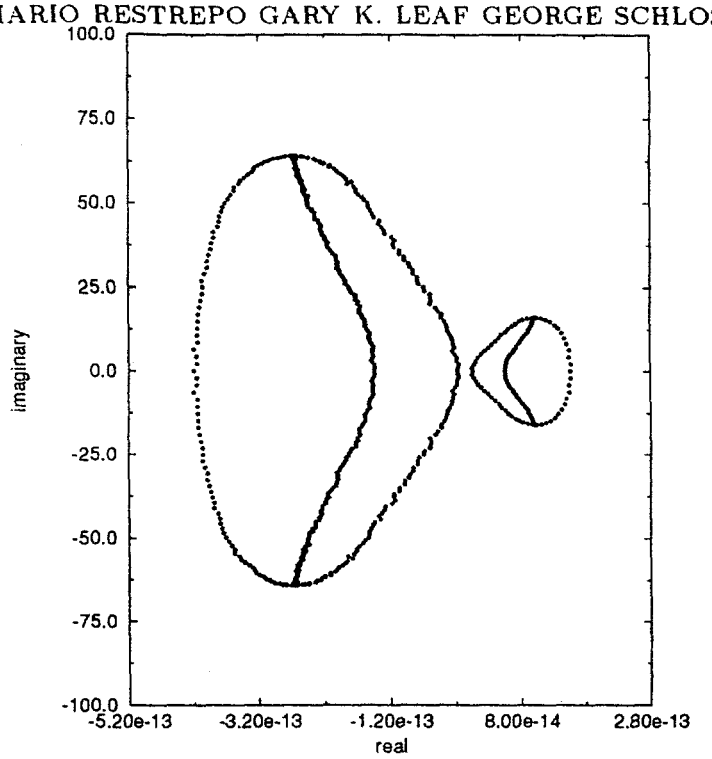

FIGURE 11B. ES real part reversal of the spectrum of $\frac{d}{dx}$; for $p = 6$ and $p = 8$ with periodic boundary conditions (triangles); for $p = 6$ and $p = 8$ with boundary constraints removed (circles)

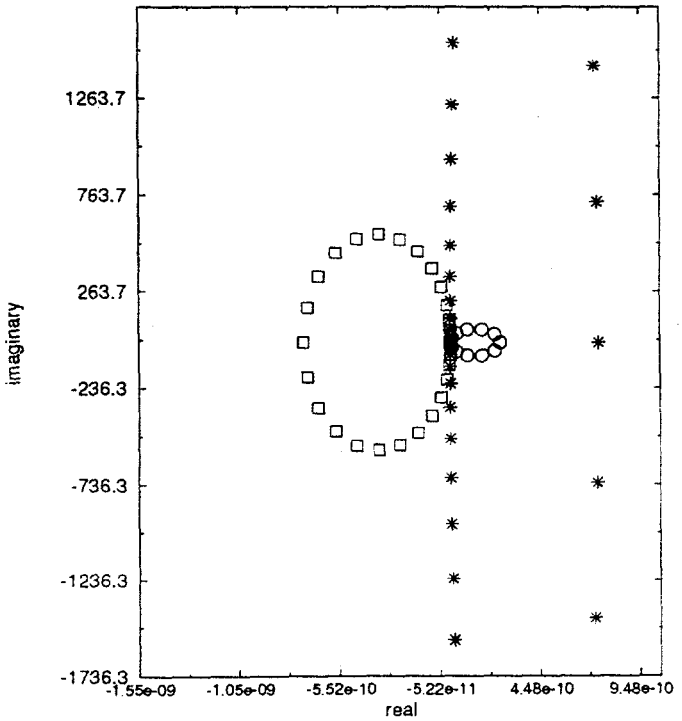

FIGURE 12. ES spectrum of $\frac{d^3}{dx^3}$; for $p = 4$ (circles), $p = 5$ (squares), and part of $p = 6$ (stars)

In summary, we have shown that common differential operators may be approximated

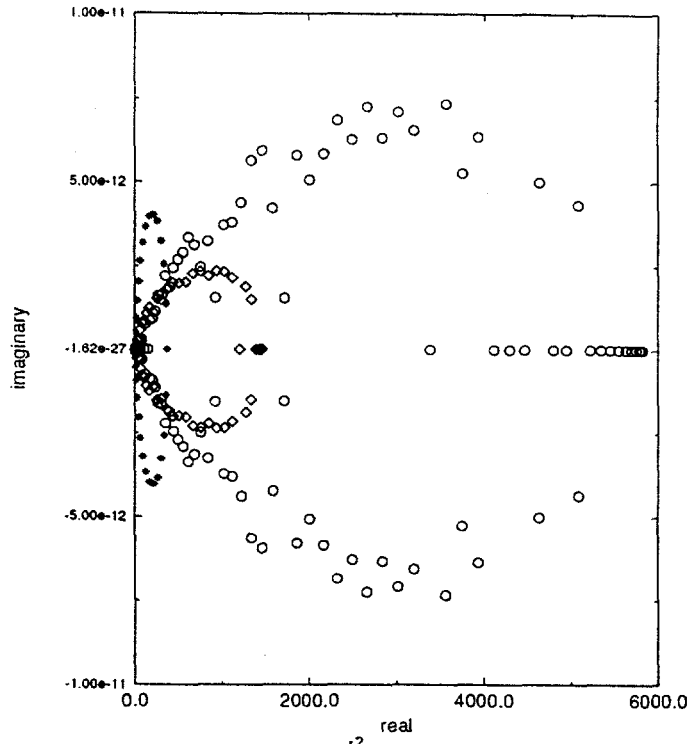

FIGURE 13A. ES spectrum of $\frac{d^2}{dx^2}$; for $p = 5$ (stars), $p = 6$ (squares), $p = 7$ (circles)

TABLE 4. Real part of eigenvalues for $\frac{d^2}{dx^2}$ divided by $4\pi^2$ for increasing resolution p. $DN = 6$

$p = 4$	$p = 6$	$p = 8$
1.1518884962509D-14	2.7645323910020D-13	0.0D0
1.0033162940157	1.0000135268157	1.0000000529814
4.1847329915128	4.0008582644240	4.0000033890207
10.666776606377	9.0096362703930	9.0000385683104
22.726823972803	16.053060704248	16.000216429062
41.582358732169	25.197220008678	25.000824274322

using wavelets. In light of other studies that compare several spectral approximations to the above operators [**16**], the wavelet aproximations compare very favorably. We examined two methods to obtain the wavelet approximation to differential operators, presuming that in wavelet applications either technique could arise. We found that for low p or low-order differential operators, the method's performance is similar. However, care must be exercised in interpreting results from the ES method when applied to problems with large p or large order in the differential operator.

Taking the spectrum calculation of $\frac{d}{dx}$ as an example of the general case, we find that the ES method always yields complex conjugate eigenvalues, which is not the case for the

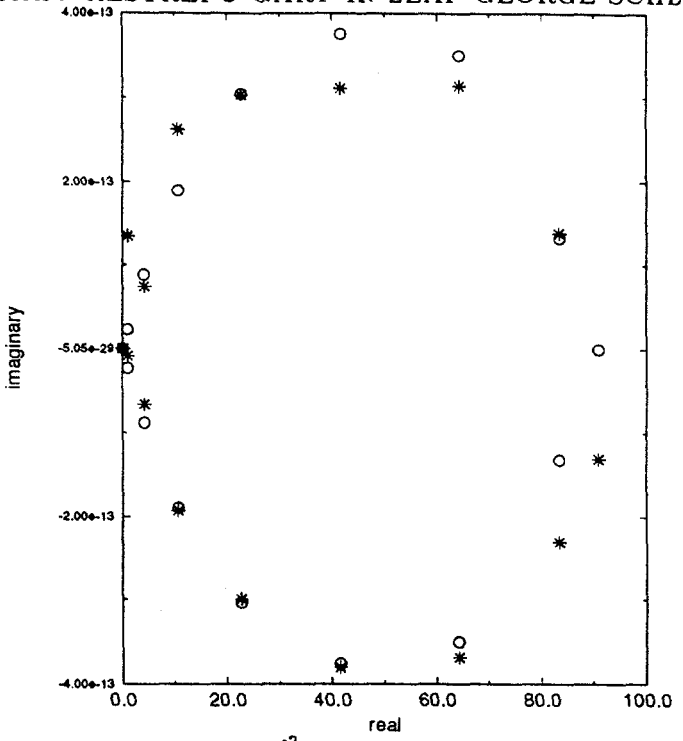

FIGURE 13B. Spectrum of $\frac{d^2}{dx^2}$ for $p = 4$ and $DN = 6$. EC (stars), ES (circles)

EC method. For the EC method, using special care in how the alternating series is added, the accuracy of the eigenvalue calculation is limited by how well the Λ's are computed. With single as well as double-precision arithmetic we find that the eigenvalues of $\Omega^{0,1}$ are always complex. Since the size of the real part of the eigenvalues is comparable to machine precision, it was not possible to asertain numerically whether the real part of the spectrum decreased uniformly to a particular set of values, or zero, as the machine precision and p were increased.

APPENDIX

Tables of Connection Coefficients.

Connection coefficients: 2-tuples for p=0, N=6. Computed in double precision on a Sun Sparc1 workstation using LAPACK solver routines.

$$\Lambda_1^{0,1} = -3.4246575342471D-04$$
$$\Lambda_2^{0,1} = -1.4611872146119D-02$$
$$\Lambda_3^{0,1} = +0.14520547945205$$
$$\Lambda_4^{0,1} = -0.74520547945205$$
$$\Lambda_5^{0,1} = -3.2049276679778D-15$$
$$\Lambda_6^{0,1} = +0.74520547945206$$
$$\Lambda_7^{0,1} = -0.14520547945205$$
$$\Lambda_8^{0,1} = +1.4611872146119D-02$$
$$\Lambda_9^{0,1} = +3.4246575342476D-04$$

residual = 1.9680979936043D-16
for the least-squares solution of the overdetermined system.

$$\Lambda_1^{1,1} = +5.3571428571412D-03$$
$$\Lambda_2^{1,1} = +0.11428571428572$$
$$\Lambda_3^{1,1} = -0.87619047619048$$
$$\Lambda_4^{1,1} = +3.3904761904762$$
$$\Lambda_5^{1,1} = -5.2678571428572$$
$$\Lambda_6^{1,1} = +3.3904761904762$$
$$\Lambda_7^{1,1} = -0.87619047619048$$
$$\Lambda_8^{1,1} = +0.11428571428571$$
$$\Lambda_9^{1,1} = +5.3571428571430D-03$$

residual = 1.1362438767648D-16

$$\Lambda_1^{2,0} = +\,5.3571428571412D-03$$
$$\Lambda_2^{2,0} = +\,0.11428571428572$$
$$\Lambda_3^{2,0} = -\,0.87619047619048$$
$$\Lambda_4^{2,0} = +\,3.3904761904762$$
$$\Lambda_5^{2,0} = -\,5.2678571428572$$
$$\Lambda_6^{2,0} = +\,3.3904761904762$$
$$\Lambda_7^{2,0} = -\,0.87619047619048$$
$$\Lambda_8^{2,0} = +\,0.11428571428571$$
$$\Lambda_9^{2,0} = +\,5.3571428571430D-03$$

residual = 1.1362438767648D-16

Tables of two-tuples and three-tuples will be made available as ASCII files. Information on how to obtain connection coefficients tables will be available after September 1994. Send mail to `wavelets@mcs.anl.gov`.

REFERENCES

1. C. Chui, *An Introduction to Wavelets*, Academic Press, New York, 1992.

2. I. Daubechies, *Ten Lectures on Wavelets*, Regional Conference Series in Applied Mathematics, vol. 61, SIAM, Philadelphia, 1992.

3. Y. Meyer, *Ondelettes et Operateurs I*, Editeurs des Sciences et des Arts, Hermann, 1990.

4. J. S. Xu and W. C. Shann, *Galerkin-Wavelet Methods for Two-Point Boundary Value Problems*, preprint, 1992.

5. G. Beylkin, R. Coifman and V. Rokhlin, *Fast Wavelet Transforms and Numerical Algorithms I*, Communications on Pure and Applied Mathematics **44** (1991), 141–183.

6. G. Battle, *A Block Spin Construction of Ondelettes, Part I: Lemarié Functions*, Communications in Mathematical Physics **110** (1987), 601–615.

7. A. Latto, H. L. Resnikoff and E. Tenenbaum, *The Evaluation of Connection Coefficients of Compactly Supported Wavelets*, preprint, 1991.

8. W. Press, S. Teukolsky, W. Vetterling and B. Flannery, *Numerical Recipes in Fortran*, in The Art of Scientific Computing, Cambridge University Press, Cambridge, 1992.

9. W. Sweldens and R. Piessens, *Quadrature Formulae for the Calculation of the Wavelet Decomposition*, preprint, 1991.

10. W. Rudin, *Real and Complex Analysis*, McGraw-Hill, Inc., New York, 1987.

11. C. Canuto, M. Y. Hussaini, A. Quarteroni and T. A. Zang, *Spectral Methods in Fluid Dynamics*, Springer Series in Computational Physics, Springer-Verlag, New York, 1988.

12. G. Beylkin, *On the Representation of Operators in Bases of Compactly Supported Wavelets*, SIAM Journal of Numerical Analysis **6** (1992), 1716–1740.

13. S. Qian and J. Weiss, *Wavelets and the Numerical Solution of Partial Differential Equations* , Aware Technical Report AD920318, 1992.

14. P. J. Davis, *Circulant Matrices*, John Wiley and Sons, New York, 1979.

15. E. Anderson, et al., *LAPACK User's Guide*, Society for Industrial and Applied Mathematics, Philadelphia, PA, 1992.

16. L. N. Trefethen and M. R. Trummer, *An Instability Phenomenon in Spectral Methods*, SIAM Journal of Numerical Analysis **24** (1987), 1008–1023.

MATHEMATICS AND COMPUTER SCIENCE DIVISION, ARGONNE NATIONAL LABORATORY, ARGONNE, IL 60439 U.S.A

E-mail address: restrepo@mcs.anl.gov

MATHEMATICS AND COMPUTER SCIENCE DIVISION ARGONNE NATIONAL LABORATORY, ARGONNE, IL 60439 U.S.A.

E-mail address: leaf@mcs.anl.gov

DEPARTMENT OF MATHEMATICS, JOHNS HOPKINS UNIVERSITY, BATIMORE, MD 21218 U.S.A.

E-mail address: schlossn@mcs.anl.gov